Monthly Notices of the ROYAL ASTRONOMICAL SOCIETY

MNRAS **507,** 3564–3571 (2021) https://doi.org/10.1093/mnras/stab2272
Advance Access publication 2021 August 6

Collisional cooling of primordial and interstellar media by H_2

D. R. Flower [1★], G. Pineau des Forêts,[2,3] P. Hily-Blant [4], A. Faure [4], F. Lique[5] and T. González-Lezana[6]

[1]*Physics Department, Durham University, Durham DH1 3LE, UK*
[2]*Institut d'Astrophysique Spatiale, CNRS, Université de Paris-Saclay, F-91405 Orsay, France*
[3]*LERMA, Observatoire de Paris, PSL University, CNRS, Sorbonne Université, F-75014 Paris, France*
[4]*IPAG (UMR 5571), CNRS, Université de Grenoble Alpes, F-38000 Grenoble, France*
[5]*IPR, CNRS, Université de Rennes, F-35000 Rennes, France*
[6]*Instituto de Física Fundamental, IFF-CSIC, Serrano 123, E-28006 Madrid, Spain*

Accepted 2021 August 1. Received 2021 July 22; in original form 2021 June 9

ABSTRACT

We have computed the rate of collisional cooling of a gas by H_2 molecules under conditions appropriate to the primordial and interstellar media. We incorporated the results of recent calculations of the rate coefficients for collisional excitation of H_2 by H and H^+, which are essential to a reliable evaluation of the *ortho*:*para* H_2 ratio and the cooling rate. Comparison is made with the results of previous calculations of the cooling function. The data are made available for grids of values of the kinetic temperature, density, H:H_2 ratio, and the fractional abundance of H^+, together with a programme to perform linear interpolation of the data sets for any given set of values of these parameters, within the ranges of the grids.

Key words: atomic data – molecular data – molecular processes – shock waves – cosmology: miscellaneous.

1 INTRODUCTION

It is recognized that the formation of the first condensations in the primordial medium, through gravitational contraction, is necessarily mediated by molecular hydrogen, which provides the only significant means of evacuating the heat generated by the contraction. This recognition has led to studies of the chemical and physical processes that take place in the course of the expansion of the primordial medium, which determine the initial conditions of the contraction process (Galli & Palla 1998; Flower & Pineau des Forêts 2000; Glover & Abel 2008; Coppola et al. 2017; Walker, Porter & Stancil 2018).

The absence of dust in the primordial gas and the low density of the medium imply that molecular hydrogen can form only through gas-phase binary reactions; this situation is in sharp contrast to the formation of H_2 at the present epoch, which is understood to occur almost exclusively on dust grains, which play the role of a third body in reactions between H atoms on their surfaces. In the primordial gas, on the other hand, H_2 forms in the reactions[1]

$$\mathrm{H} + \mathrm{H}^+ \rightarrow \mathrm{H_2}^+ + h\nu$$

followed by

$$\mathrm{H_2}^+ + \mathrm{H} \rightarrow \mathrm{H}^+ + \mathrm{H_2}$$

or

$$\mathrm{H} + \mathrm{e}^- \rightarrow \mathrm{H}^- + h\nu$$

followed by

$$\mathrm{H}^- + \mathrm{H} \rightarrow \mathrm{e}^- + \mathrm{H_2},$$

where, in the first reaction of each pair, stabilization of the product is achieved through the emission of a photon, which is an inherently slow process. Consequently, the fractional abundance of H_2 does not attain its peak value of $n(H_2)/n_H \approx 10^{-6}$, where $n_H = n(H) + 2n(H_2) + n(H^+)$, until a redshift $z \approx 100$ (expansion time $t \approx 10$ Myr). It has been shown that even such a small initial fractional abundance of H_2 is sufficient to ensure thermal stabilization of a subsequent gravitational contraction (Flower & Pineau des Forêts 2001).

While cooling of the medium by H_2 is critical for the formation of the first condensations, it is negligible in the context of the adiabatic expansion of the primordial gas – a fact that has perhaps been inadequately appreciated. Under conditions appropriate to the early Universe, H_2 can contribute to the heating, rather than the cooling, of the gas (Puy et al. 1993; Flower & Pineau des Forêts 2000). In practice, the kinetic temperature of the gas is determined, for $z \gtrsim 300$, by the interaction with the cosmic background radiation field, through Thomson scattering of photons on the electrons. For $z \lesssim 300$, the kinetic temperature is determined by the adiabatic expansion of the medium – until re-ionization occurs, following the formation of the first (Pop III) stars. Thus, the details of collisional and spontaneous radiative population transfer of the rovibrational levels of H_2 are insignificant when calculating the kinetic temperature profile of the adiabatically expanding primordial gas. Furthermore, the H_2 level populations are thermalized to the cosmic background radiation temperature. On the other hand, once condensations begin to contract gravitationally, the matter density increases relative to the radiation density, and collision-induced transitions assume importance, relative to transitions induced by the background radiation field.

★ E-mail: david.flower@durham.ac.uk

[1]The production of H_2 through the formation of HeH^+ as an intermediary has also been proposed (Courtney et al. 2020). This mechanism could enhance the fractional abundance of H_2 by no more than the He:H elemental abundance ratio, i.e. by no more than 8 per cent.

A particularity of H_2 is its *ortho* (J odd) and *para* (J even) dichotomy, where J is the rotational quantum number. Although radiative transitions between *ortho* and *para* levels can occur, their probabilities are extremely low. For example, the Einstein A-coefficient for $v = 0, J = 1 \rightarrow v' = 0, J' = 0$ transition is $A_{1\rightarrow0} = 2 \times 10^{-21}$ s^{-1} (Pachucki & Komasa 2008), which results in radiative transitions being negligible within the lifetime of the Universe. In practice, the *ortho*:*para* H_2 ratio is determined by nuclear-spin-changing collisions with hydrogen atoms and protons or proton-transferring ions. As will be seen in Section 3, proton collisions dominate transitions between the levels $v = 0, J = 1$, and $J = 0$ at low temperatures. When the proton density becomes so low that the time-scale for these transitions exceeds the expansion time-scale, freeze-out of the relative $J = 1$ and $J = 0$ level populations occurs,[2] at $z \approx 10$.

In addition to the formation of the first gravitationally bound structures, radiative cooling by hydrogen molecules can be significant, or even dominant, in molecular regions of interstellar media that have been heated to temperatures $T \gtrsim 100$ K by a radiation field or a shock wave, for example. By contrast, the kinetic temperature in quiescent molecular clouds is too low for collisional excitation of H_2 to be a significant cooling process, owing to its large rotational constant. Under interstellar conditions, the *ortho*:*para* ratio can be significantly affected by the formation of H_2 on grains, whose rate may be comparable with the rates of other population transfer mechanisms, particularly at low temperatures.

The aim of the present study is to demonstrate the consequences of introducing recently calculated rate coefficients for excitation of H_2 by the perturbers H and H^+ into computations of the cooling rate, in circumstances where collisions dominate population transfer. Our intention is not to model specific media, in which population transfer might also be mediated by other processes. As will be seen from the results in Section 3, the principal effect of incorporating new rate coefficients for H–H_2 and H^+–H_2 collisions is to change the *ortho*:*para* ratio, through nuclear-spin-changing reactions, and thence the cooling rate. The *ortho*:*para* ratio is not modified by radiative transitions, which – as has already been mentioned – are highly forbidden. Thus, our results represent the case in which collisions with the dominant perturbers, H, He, H_2, H^+, and e^-, rather than interactions with a radiation field, determine the populations of the rovibrational level of H_2 and the local cooling rate.

In Section 2, we describe our calculations of the rate of cooling by H_2 for a range of parameters that is relevant to both the primordial and interstellar media. The results of these calculations are presented and discussed in Sections 3 and 4. Our conclusions are summarized in Section 5.

2 CALCULATIONS OF THE H_2 COOLING FUNCTION, W

We define the H_2 cooling function as the rate of radiative cooling per H_2 molecule, that is

$$W(\mathrm{H_2}) = \frac{1}{n(\mathrm{H_2})} \sum_{vJ,v'J'} (E_{vJ} - E_{v'J'}) n_{vJ} A(vJ \rightarrow v'J')$$

for $E_{vJ} > E_{v'J'}$, where E_{vJ} are the energies of the rovibrational levels of H_2 in its ground electronic state. When calculating the level populations, n_{vJ} (cm^{-3}), we assume that collisional excitation of H_2 by the perturbers H, He, H_2, H^+, and e^- is followed either by collisional de-excitation or by spontaneous radiative decay with probability A (s^{-1}); W is calculated in units of erg s^{-1} (10^{-7} W). When, as here, interactions with a radiation field are neglected, the level populations are not usually in local thermodynamic equilibrium, and the key to an accurate calculation of the cooling function is reliable values of the rate coefficients for collisional excitation and de-excitation of the molecule.

The expression above for the cooling rate, $W(H_2)$, assumes that the photons that are emitted in spontaneous rovibrational transitions escape from the medium, rather than being reabsorbed. The rovibrational spectrum of H_2 is quadrupolar, and the transition probabilities, $A \lesssim 10^{-6}$ s^{-1}, i.e. typically 14 orders of magnitude smaller than dipolar electronic transitions in the Lyman and Werner ultraviolet bands (Abgrall & Roueff 1989).[3] As shown by Puy et al. (1993), the Doppler shift associated with the expansion of the early Universe ensures that these photons are not reabsorbed. A possible exception is the cores of collapsing condensations (Ripamonti & Abel 2004); but the density in such cases is so large that the H_2 rovibrational level populations are given by a Boltzmann distribution at the local kinetic temperature (Section 4).

Since our earlier study (Le Bourlot, Pineau des Forêts & Flower 1999), new calculations of the rate coefficients for rovibrational excitation of H_2 by H and H^+ have become available. These processes are particularly important, as nuclear-spin-changing (i.e. reactive) collisions with H and H^+ are responsible for the interconversion of the *ortho* and *para* forms[4] of H_2. For excitation by H, we used rate coefficients that are an extension of previous work (Lique 2015), with a finer temperature grid. These data cover the temperature range 100 K $< T <$ 5000 K and 54 levels of H_2 with energies up to E ($v = 3, J = 8$) = 21911 K. Rovibrational excitation by He was included, using the same rate coefficients as Le Bourlot et al. (1999), extending to levels approximately 20 000 K above the ground state, $v = 0$, $J = 0$. We note that collisions with He are of secondary importance, owing to its fractional abundance being lower than that of H and/or H_2 and the absence of ortho $\leftrightarrow$ para interconversion. For excitation by H^+, we use the data of González-Lezana, Hily-Blant & Faure (2021) for the temperature range 5 K $< T <$ 3000 K and 26 levels of H_2 with energies up to E ($v = 2, J = 3$) = 12550 K.

Following Flower et al. (2000), we allow for excitation not only by *para*-H_2($J = 0$) but also by *ortho*-H_2($J = 1$). Their data remain the most complete sets of ab initio calculations of rate coefficients for the rovibrational excitation of H_2 by H_2, comprising levels up to approximately 20 000 K above the ground state; they are in good agreement with subsequent calculations by Lee et al. (2008) of the rate coefficients for rotational transitions $J - J' = 2$, $2 \leq J \leq 8$, within the vibrational ground state, $v = 0$. We have also verified that the more extensive set of rate coefficients for rotational transitions, derived by Wan et al. (2018), yield values of the cooling function that are consistent with those obtained using the data of Flower et al. (2000) (see Fig. 1). We note that Montero, Tejeda & Fernández (2020) have made a limited comparison, for four rotationally inelastic transitions, of the rate coefficients computed by Wan et al. (2018) with

[2]In the limit of freeze-out, the *ortho*:*para* ratio becomes constant and equal to the ratio of the populations of the $J = 1$ (*ortho*) and $J = 0$ (*para*) rotational levels, but, in general, the *ortho*:*para* ratio must be evaluated from summations of the population densities of odd- and even-J levels.

[3]In the interstellar context, elaborate models of photon-dominated regions (PDRs), such as the Meudon PDR code (Le Petit et al. 2006), have been developed in which all relevant heating and cooling processes are taken into account, with proper allowance for radiative transfer in the ultraviolet lines.

[4]Proton-exchange collisions with other species, such as H_3^+, can also play a role, particularly in the interstellar medium.

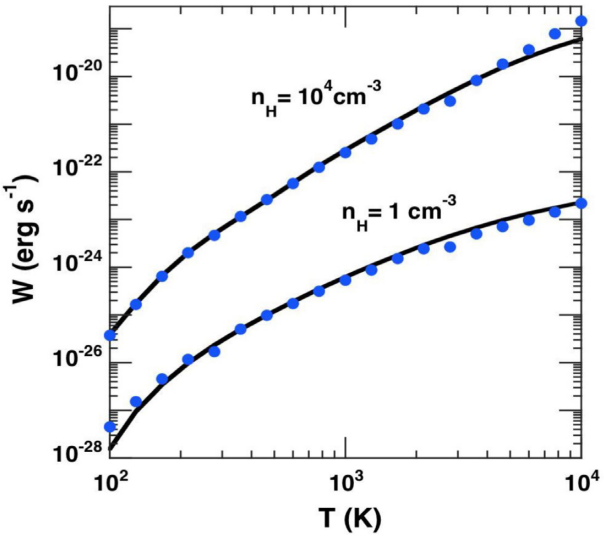

Figure 1. The rate of cooling of molecular gas as a function of temperature, T, calculated at two densities and adopting the H_2–H_2 rate coefficients of Le Bourlot et al. (1999) (full black curves) or Wan et al. (2018) (blue data points).

empirically derived values and found the theoretical rate coefficients to be lower than their measurements for temperatures 20 K $< T <$ 295 K. In a more recent study, Hernández et al. (2021) compared experimental and theoretical rate coefficients for three rotationally inelastic transitions, induced by either $H_2(J = 0)$ or $H_2(J = 1)$, and found that the data adopted in the present calculations are generally in better accord with their measurements than those of Wan et al. (2018).

Rotationally inelastic collisions with electrons were also taken into account by means of rate coefficients for 10 K $< T <$ 4000 K and the rotational transitions $J - J' = 2$, $2 \leq J \leq 5$, derived from the empirical excitation cross sections of England, Elford & Crompton (1988); charge neutrality requires that $n(e^-) = n(H^+)$. The rates of these transitions, induced by electrons, become comparable with their rates, induced by protons, for $T \gtrsim 1000$ K, but, at these high temperatures, collisions with H and/or H_2 tend to dominate.

For kinetic temperatures in the above ranges, the rate coefficients, q (cm^3 s^{-1}), for de-excitation of H_2 in collisions with H and H^+ were evaluated by means of cubic-spline interpolation of the data points; the rate coefficients for excitation were derived from the detailed-balance relation,

$$g_{I'} g_{J'} q(v'J' \rightarrow vJ) = g_I g_J q(vJ \rightarrow v'J') \exp - \frac{(E_{vJ} - E_{v'J'})}{k_B T},$$

where $g_I = 2I + 1$ is the nuclear-spin statistical weight (3 for odd J and 1 for even J) and $g_J = 2J + 1$ is the rotational degeneracy. At temperatures greater than the upper limits, we adopt the values calculated at the highest temperature for which the collision data are available. Where no data are available, the corresponding rate coefficients are set equal to zero. This assumption is potentially most significant at high temperatures and for collisions with H^+: when the number of H_2 levels included in the calculation of their population densities exceeds 26, the H^+–H_2 rate coefficients for transitions to or from higher levels are taken equal to zero. However, we note that H^+ collisions are most important at low, not high, temperatures.

The parameters of the cooling function were taken to be the fractional H^+ density, $x(H^+) = n(H^+)/n_H$, the ratio of the densities of H and H_2, $n(H)/n(H_2)$, the total proton density, $n_H = n(H) + 2n(H_2) + n(H^+)$, and the kinetic temperature, T. The population densities, n_{vJ}, of the rovibrational levels of H_2 were calculated by integrating[5] the coupled differential equations for the rates of population transfer, dn_{vJ}/dt, with respect to time, t; the upper limit to t was taken to be 9×10^{16} s, which is comparable with the age of the Universe. We note that this approach implies that the initial *ortho*:*para* H_2 ratio cannot be adopted as a parameter of the computations, as was assumed by Le Bourlot et al. (1999), given that the *ortho*:*para* ratio changes as the integration proceeds towards equilibrium, owing to nuclear-spin-changing collisions with H and H^+.[6]

Table 1. The parameters of the cooling function and their grid of values; log is base 10.

Parameter	Lower limit	Upper limit	Step size
log T (K)	2.000	4.000	0.111
log n_H (cm^{-3})	0	6	1
log[n(H)/n(H$_2$)]	− 6	6	2
log[n(H$^+$)/n_H]	− 8	− 1	1

3 RESULTS

The cooling function was evaluated for the following ranges of the independent parameters: 100 K $\leq T \leq$ 10 000 K; 1 cm^{-3} $\leq n_H \leq 10^6$ cm^{-3}; $10^{-6} \leq n(H)/n(H_2) \leq 10^6$; $10^{-8} \leq x(H^+) \leq 10^{-1}$ (see Table 1). For the purposes of illustration of the results, we consider $n_H = 1$ cm^{-3} and $n_H = 10^4$ cm^{-3} as representative of low- and high-density gas, respectively; both 'atomic' and 'molecular' gas, corresponding to $n(H)/n(H_2) = 10^6$ and $n(H)/n(H_2) = 10^{-2}$, respectively, and $x(H^+) = 10^{-4}$ or $x(H^+) = 10^{-2}$. The He abundance, $x(He) = n(He)/n_H$ was taken equal to either 0.10, representative of the interstellar medium of the present epoch (Anders & Grevesse 1989), or 0.08, its primordial value (Pitrou et al. 2018). Even in the extreme case of an atomic gas [$n(H)/n(H_2) = 10^6$] of low ionization ($x(H^+) = 10^{-8}$) and low temperature ($T \approx 10^2$ K), the difference between the cooling rates for these two values of x(He) did not exceed 15 per cent. Therefore, a complete set of data was computed only for $x(He) = 0.10$. A subset of calculations was performed including all rovibrational levels with $E_{vJ} \leq 1.0 \times 10^4$ K (18 levels) and $E_{vJ} \leq 1.5 \times 10^4$ K (32 levels), in addition to $E_{vJ} \leq 2.0 \times 10^4$ K (49 levels), for which the complete grid was computed, in order to establish the convergence of the results with respect to the number of levels.

3.1 Influence of the new collision rates

We consider first the significance of the revisions to the rate coefficients for collisional energy transfer.

(i) In molecular gas, collisional excitation of H_2 (the 'target' molecule) by H_2 (the 'perturber' molecule) becomes important. Le Bourlot et al. (1999) considered that $H_2(J = 0)$ was the sole perturber, taking its density to be equal to the total density of H_2. As mentioned

[5]The method of Gear (1971) for solving 'stiff' differential equations was used, taking into account population transfer by spontaneous radiative transitions and inelastic collisions.

[6]For the lowest density, $n_H = 1$ cm^{-3}, and lowest degree of ionization, $x(H^+) = 10^{-8}$, considered, the *ortho*:*para* ratio and hence the cooling function do not attain their steady-state values at the lowest temperatures, $T \approx 10^2$ K, but, in this case, the corresponding cooling rates are negligible and the combination of low density and ionization is not of practical significance.

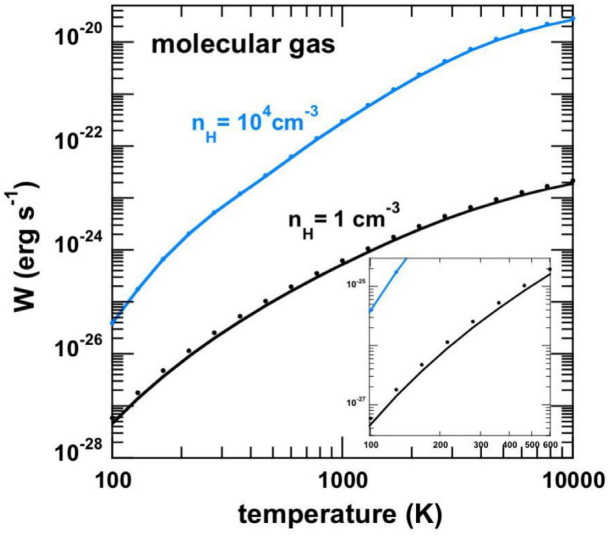

Figure 2. The rate of cooling of molecular gas as a function of temperature, T, calculated at two densities and assuming collisions with *para*-$H_2(J = 0)$ (full curves) or *ortho*-$H_2(J = 1)$ (data points); $x(H^+) = 10^{-4}$ in this calculation. The inset shows the cooling function for 100 K $\leq T \leq$ 600 K on an expanded scale.

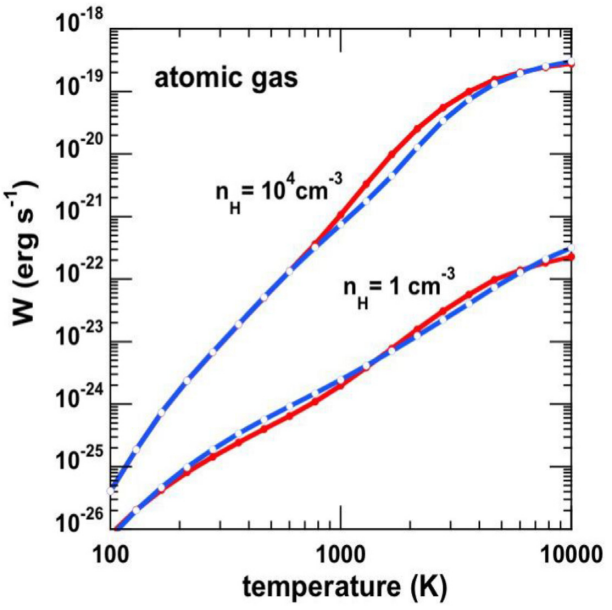

Figure 3. The rate of cooling of atomic gas as a function of temperature, calculated at two densities and adopting either the same H–H_2 and H^+–H_2 rate coefficients as Le Bourlot et al. (1999) (broken blue curves) or their present values (full red curves); $x(H^+) = 10^{-2}$ in this calculation.

above, we now include excitation by both $H_2(J = 0)$ and $H_2(J = 1)$, taking their densities equal to the calculated densities of *para*- and *ortho*-H_2, respectively, and it is instructive to investigate the sensitivity of the cooling rate to the introduction of $H_2(J = 1)$ as a perturber.

In Fig. 2 are compared the extreme cases in which the perturber molecule is assumed to be either $H_2(J = 0)$ or $H_2(J = 1)$, with the density of each being taken equal to $n(H_2)$; this calculation comprised the 18 lowest energy levels of H_2 ($E_{vJ} \leq 1.0 \times 10^4$ K), and we consider the molecular case, for which excitation by H_2 is important, relative to excitation by the other perturbers. As is clear from the figure, the cooling rate is insensitive to the rotational state of the perturber H_2 molecule ($J = 0$ or $J = 1$): the maximum discrepancy between these extreme cases is 30 per cent.

The main distinction between $H_2(J = 0)$ and $H_2(J = 1)$ as perturbers is associated with the difference in the long-range forms of the interaction potentials for $J = 0$ and $J > 0$, which becomes significant at low collision energies and kinetic temperatures (cf. Wan et al. 2018) – lower, in fact, than those for which excitation by H_2 is a significant contributor to the cooling process. Furthermore, as the target molecule assumes both *ortho* and *para* forms, the *ortho*–*para* combination of perturber and target molecules is common to excitation by both $H_2(J = 0)$ and $H_2(J = 1)$.

We note that, in the case of collisions between identical molecules, the distinction between 'perturber' and 'target' molecules is a convenient artefact that would have to be abandoned were the contribution of H_2–H_2 collisions to the cooling rate found to be sensitive to their *ortho* and *para* forms.

(ii) In view of the significance of collisions of H and H^+ with H_2 in establishing the *ortho*:*para* ratio, we compare (in Fig. 3) the present cooling rates with those calculated using the H–H_2 and H^+–H_2 rate coefficients of Le Bourlot et al. (1999). The 'atomic' case is considered, with $x(H^+) = 10^{-2}$, in order to maximize the significance of H and H^+ collisions; 32 levels of H_2 were included in these calculations. We see that, at the higher density of $n_H = 10^4$ cm^{-3}, differences in the cooling rates, attaining a factor of approximately 2.5, occur for $T \approx 2000$ K. At the lower density of $n_H = 1$ cm^{-3}, the differences in the cooling rates are smaller but extend over a wider temperature range.

At temperatures $T \lesssim 100$ K, only the $J = 0$ and $J = 1$ rotational levels of the vibrational ground state are significantly populated, and transfer between them is dominated by collisions with H^+. Consequently, the *ortho*:*para* ratio tends towards

$$\frac{n(J=1)}{n(J=0)} = 9 \exp -\frac{170.5}{T}$$

its value in thermodynamic equilibrium; 170.5 K is the difference in energy between the $J = 1$ and $J = 0$ levels. At high temperatures, $T \gtrsim 1000$ K, where collisions with H dominate, the *ortho*:*para* ratio tends towards its statistical value of 3.

3.2 Influence of the number of H_2 levels

Fig. 4 illustrates the effects of increasing the number of H_2 levels, from 32 ($E_{vJ} \leq 1.5 \times 10^4$ K) to 49 ($E_{vJ} \leq 2.0 \times 10^4$ K). In molecular gas, the cooling rates are practically identical. On the other hand, in atomic gas, increasing the number of levels leads to higher cooling rates at temperatures $T \gtrsim 5000$ K when $n_H = 10^4$ cm^{-3}. Reducing the number of H_2 levels further, to 18 ($E_{vJ} \leq 1.0 \times 10^4$ K), results in a lack of convergence for $T \gtrsim 3000$ K.

The final grid of values of the cooling function was generated with 49 levels of H_2, as in Le Bourlot et al. (1999).

3.3 Dependence on the physical parameters

Figs 5 and 6 illustrate the dependence of the results on the physical parameters: $x(H^+)$, $n(H)/n(H_2)$, n_H, and T. The significance of H collisions at high T and of H^+ collisions at low T is evident in Figs 5(a) and (b), respectively. The importance of collisions with H at high temperatures is again apparent in Figs 6(a) and (b), which show that, for a given value of n_H, the rate of cooling per H_2 molecule

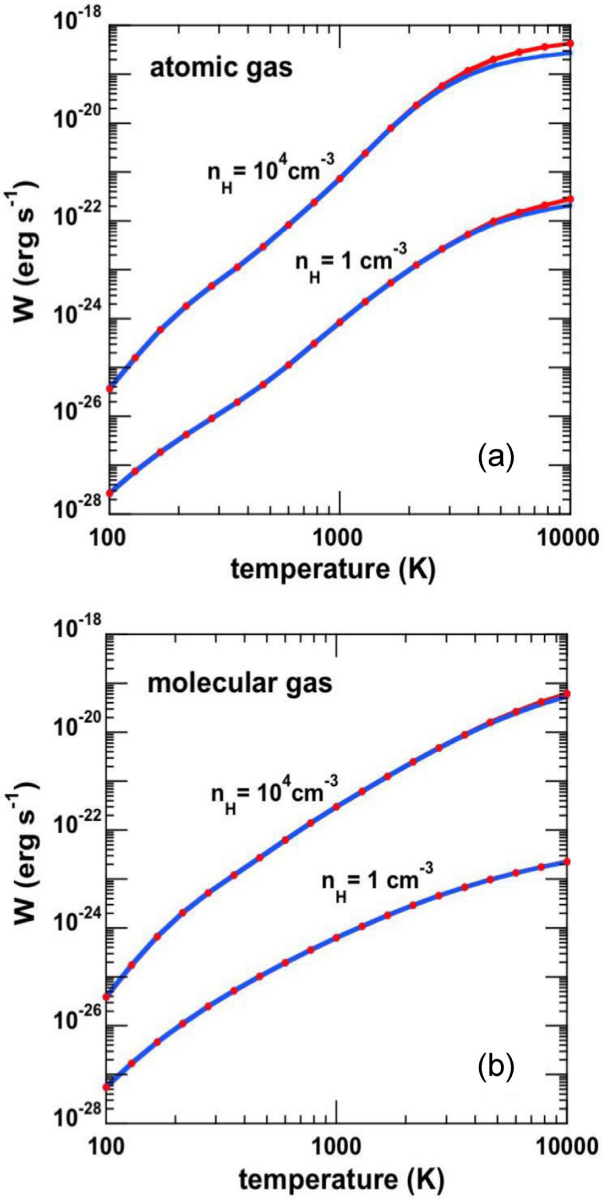

Figure 4. The rate of cooling of (a) atomic and (b) molecular gas as a function of temperature, calculated at two densities and including either 32 (full blue curves) or 49 (full red curves, with data points) levels of H_2; $x(H^+) = 10^{-4}$ in this calculation. 'Atomic' and 'molecular' gas correspond to $n(H)/n(H_2) = 10^6$ and $n(H)/n(H_2) = 10^{-2}$, respectively.

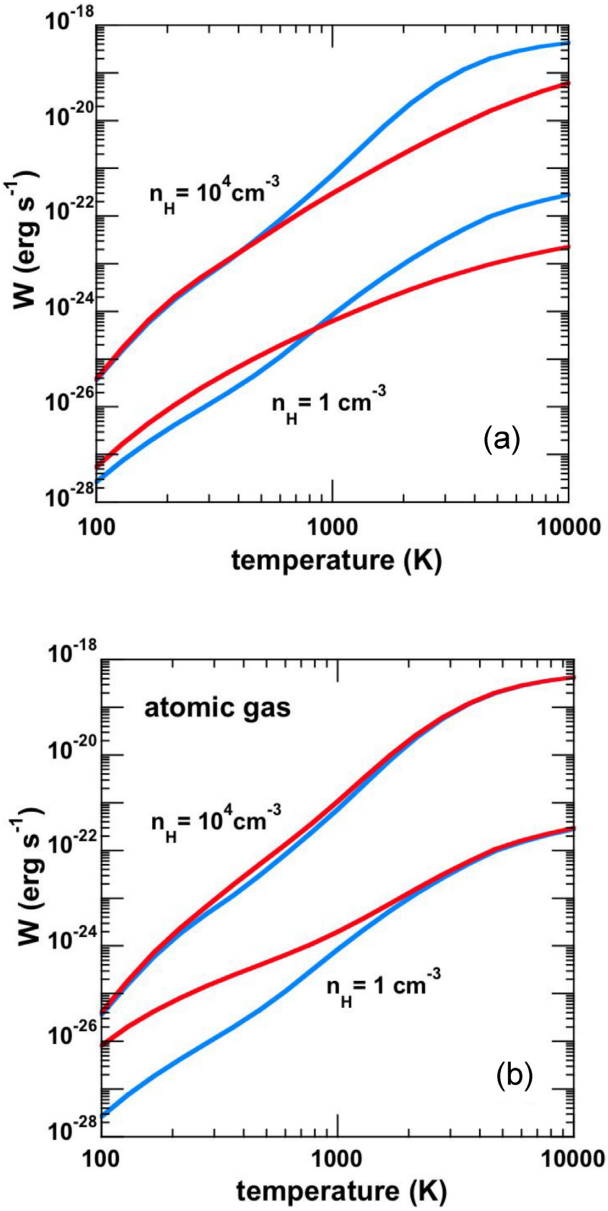

Figure 5. The rate of cooling of gas as a function of temperature, calculated at the specified densities, (a) in atomic (blue curve) and molecular (red curve) gas for $x(H^+) = 10^{-4}$; (b) in atomic gas for $x(H^+) = 10^{-4}$ (blue curve) and $x(H^+) = 10^{-2}$ (red curve).

tends to be greater in atomic than in molecular gas, owing to the higher rovibrational excitation rates in the former case.

3.4 Interpolation of the cooling rates

The cooling rate, W (erg s^{-1}), for any given set of values (within the prescribed ranges) of the four parameters [$x(H^+)$, $n(H)/n(H_2)$, n_H (cm^{-3}), and T (K)] for which it is tabulated (100 K $\leq T \leq$ 10 000 K; 1 cm^{-3} $\leq n_H \leq 10^6$ cm^{-3}; $10^{-6} \leq n(H)/n(H_2) \leq 10^6$; $10^{-8} \leq x(H^+) \leq 10^{-1}$), is derived by means of linear interpolation of the data points. The complete data set, together with a FORTRAN program (interpolation.f90, which also reads interp.inp) to perform the interpolation, are provided as supplementary online material.

4 DISCUSSION

A comparison of the present results with those of Le Bourlot et al. (1999) is made in Fig. 7. Differences attributable to the new H^+ rate coefficients are apparent at low T, in both atomic and molecular gas, and differences arising from the new H rate coefficients are evident at high T, in atomic gas.

Coppola et al. (2019) computed the dependence of the cooling function on the temperature (100 K $\leq T \leq$ 4000 K) and density (10^{-4} cm^{-3} $\leq n_H \leq 10^8$ cm^{-3}) of gas in which $x(H^+) = 2 \times 10^{-4}$ and $x(He) = 0.10$. They neglected the excitation of H_2 by H_2, and hence the appropriate comparison with our results is for the case of an atomic gas. We find that our calculations of the cooling rates in atomic gas agree well with those computed from the parameters of the fits provided by Coppola et al. (2019, table 1) for temperatures

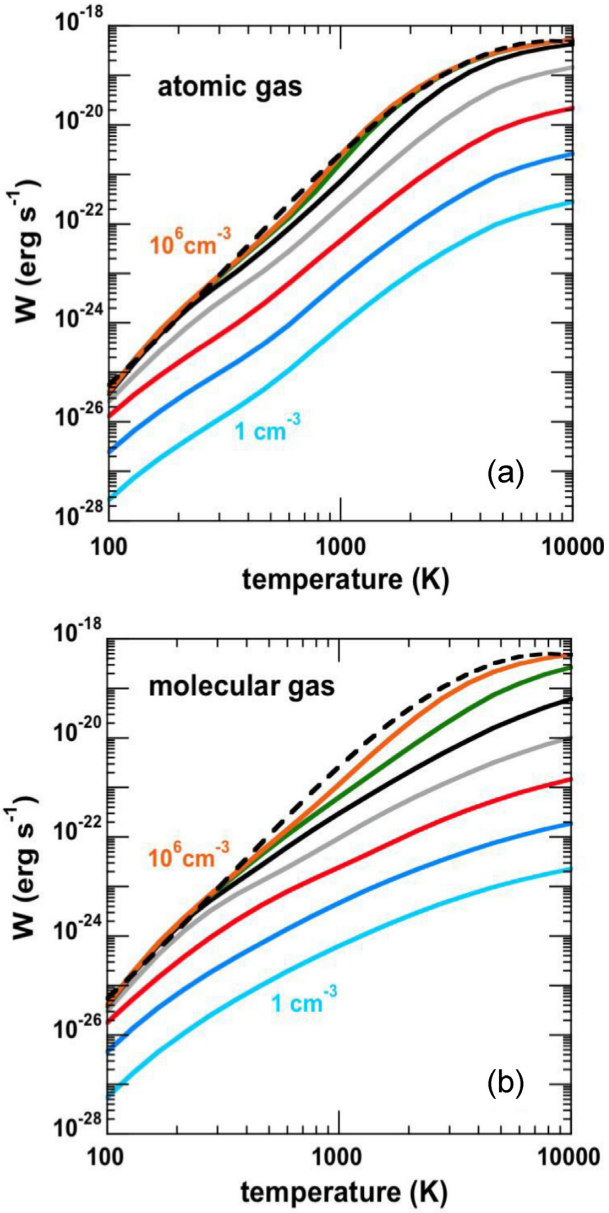

Figure 6. The rate of cooling of gas as a function of temperature, calculated for densities (from the top) $n_{\rm H} = 10^6$, 10^5, 10^4, 10^3, 10^2, 10, 1 cm^{-3} and (a) atomic gas and (b) molecular gas. The broken curve is a cubic polynomial fit, $y = \sum_{n=0}^{3} a_n x^n$, where $x = \log_{10} T$ (K) and $y = \log_{10} W$ (erg s^{-1}), which is valid only for $n_{\rm H} \geq 10^6$ cm^{-3} and 10^2 K $\leq T \leq 10^4$ K (see Table 2).

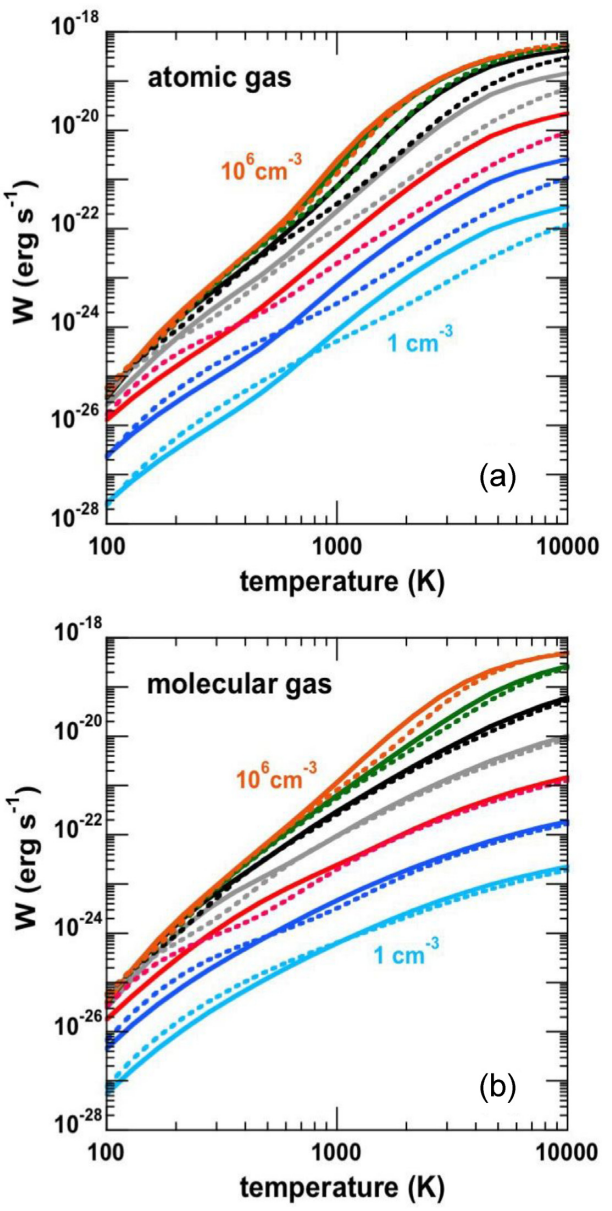

Figure 7. The rate of cooling of (a) atomic and (b) molecular gas as a function of temperature, calculated for $x(\rm H^+) = 10^{-4}$ and densities (from the top) $n_{\rm H} = 10^6$, 10^5, 10^4, 10^3, 10^2, 10, 1 cm^{-3}; the full curves are the results of the present computations, whereas the broken curves are the computations of Le Bourlot et al. (1999).

1000 K $\lesssim T \lesssim$ 4000 K (see Fig. 8). The level of agreement is less satisfactory for $T \lesssim 1000$ K, owing to differences in the values of the $\rm H^+$–$\rm H_2$ rate coefficients. Comparisons with some earlier fits to the rates of excitation of $\rm H_2$ by H and $\rm H^+$ are made in Appendix A.

The transition probabilities for spontaneous quadrupolar radiative transitions within the electronic ground state of $\rm H_2$ vary between $A \approx 10^{-11}$ s^{-1} and $A \approx 10^{-6}$ s^{-1}. Taking a characteristic rate coefficient for collisional de-excitation of 10^{-10} cm^3 s^{-1}, we see that the low-density limit, in which collisional excitation is followed by radiative decay, applies for perturber densities $\lesssim 10^{-2}$ cm^{-3}, whereas the high-density limit, in which a Boltzmann population distribution obtains, applies for perturber densities $\gtrsim 10^5$ cm^{-3} in atomic gas. Higher densities are required to attain a Boltzmann distribution of the level populations in molecular gas (see Fig. 6). The high-density limit in atomic gas is apparent in the results of Coppola et al. (2019, fig. 1), where the cooling rate per $\rm H_2$ molecule is seen to become independent of density[7] for $n_{\rm H} \gtrsim 10^5$ cm^{-3}. Similar fits are feasible at all densities in the grid for an atomic gas; the coefficients of these fits are given in Table 2. In the low-density limit, the cooling rate per $\rm H_2$ molecule at a given temperature becomes proportional to $n_{\rm H}$.

A special case is transitions between $J = 0$ and $J = 1$ in the vibrational ground state. As mentioned in Section 1, $A_{1\rightarrow 0} = 2 \times 10^{-21}$ s^{-1},

[7]In the high-density limit, when the level populations follow a Boltzmann distribution, the cooling rate per $\rm H_2$ molecule becomes dependent only on the temperature and can be fitted, to an accuracy that may be sufficient for some applications, by a cubic polynomial, $y = \sum_{n=0}^{3} a_n x^n$, where $x = \log_{10} T$ (K) and $y = \log_{10} W$ (erg s^{-1}). Such a fit is shown in Fig. 6.

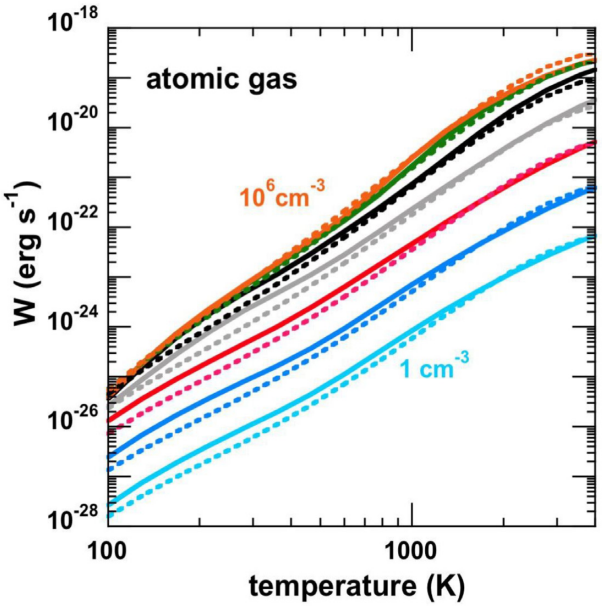

Figure 8. As Fig. 7(a) but comparing the present results (full curves) with those of Coppola et al. (2019) (broken curves).

Table 2. The coefficients of cubic polynomial fits, $y = \sum_{n=0}^{3} a_n x^n$, where $x = \log_{10} T$ (K) and $y = \log_{10} W$ (erg s^{-1}), which are valid only for 10^2 K $\leq T \leq 10^4$ K in atomic gas; $x(\mathrm{H}^+) = 10^{-4}$ and n_H is in cm^{-3}. The fits reproduce the computed data to within about 25 per cent at $T = 100$ K, where W is negligible, but to within 10 per cent at $T = 10\,000$ K, where W is large.

$\log_{10} n_\mathrm{H}$	a_0	a_1	a_2	a_3
0.0	− 21.016	1.448	− 11.550	1.508
1.0	− 19.256	1.567	− 12.269	1.632
2.0	− 18.118	1.375	− 12.898	1.431
3.0	− 22.170	2.343	− 8.815	2.440
4.0	− 19.537	3.057	− 12.134	3.182
5.0	− 18.286	2.827	− 14.274	2.944
6.0	− 19.639	2.539	− 13.203	2.644

which corresponds to a radiative lifetime of the $J = 1$ level that exceeds the age of the Universe. At temperatures $T \lesssim 100$ K, for which only the $J = 0$ and $J = 1$ levels are significantly populated, the relative population of these levels is determined by proton-exchange collisions with H^+ and tends to its value in thermodynamic equilibrium; the rate of cooling is then determined by $A_{1\rightarrow 0}$, or, in other words, the rate of cooling is negligible in the lifetime of the Universe.

An interesting consequence of collisions with H^+ determining the value of $n(J = 1)/n(J = 0)$ at low temperatures is encountered in the context of the adiabatic expansion of the primordial gas. The gas density, n_H, and fractional H^+ abundance, $x(\mathrm{H}^+)$, eventually become so low that the time-scale for population transfer through collisions with H^+ exceeds the expansion time-scale. The time-scale for *ortho* ↔ *para* interconversion is $\tau_\mathrm{op} = [k_\mathrm{op} n(\mathrm{H}^+)]^{-1}$, where $k_\mathrm{op} \approx 10^{-10}$ cm^3 s^{-1} is the interconversion rate coefficient, and $n(\mathrm{H}^+) \approx 10^{-4} n_\mathrm{H}$ and $n_\mathrm{H} \approx 10^{-3}$ cm^{-3} at freeze-out ($z \approx 10$). Thus, $\tau_\mathrm{op} \approx 3$ Gyr at freeze-out, when the expansion time-scale is approximately 0.4 Gyr. Freeze-out of $n(J = 1)/n(J = 0)$, which is effectively the *ortho*:*para* ratio, then occurs at a value that depends on the rate coefficient for $J = 0 \leftrightarrow J = 1$ collisions.

The phenomenon of freeze-out is illustrated in Fig. 9, where the *ortho*:*para* ratio is plotted as a function of redshift, adopting either

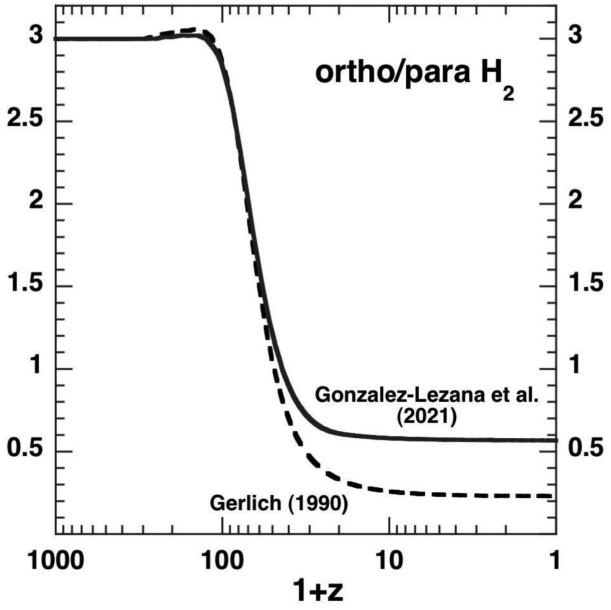

Figure 9. The *ortho*:*para* H_2 ratio computed as a function of redshift, z, using the H^+–H_2 rate coefficients of either Gerlich (1990) (broken curve) or González-Lezana et al. (2021) (full curve).

the H^+–H_2 rate coefficients of Gerlich (1990), which were used by Le Bourlot et al. (1999), or the more recent data of González-Lezana et al. (2021). For the purpose of this illustration, the cosmological model of Flower & Pineau des Forêts (2000) was adopted. It may be seen from the figure that the freeze-out value of the *ortho*:*para* ratio increases by a factor of more than 2 when the data of González-Lezana et al. (2021) are used. The computed fractional abundance of H^+ at freeze-out is $x(\mathrm{H}^+) \approx 3 \times 10^{-4}$.

5 CONCLUDING REMARKS

We have performed calculations of the rate of cooling of a gas comprising elemental hydrogen and helium by H_2 molecules, with a view to applications to both the primordial gas and the coeval interstellar medium. From the data set, the rate of cooling for given values of the kinetic temperature, density, and composition may be evaluated by linear interpolation of the data points, using the programme provided for this purpose.

Of crucial importance for the evaluation of the cooling function and the *ortho*:*para* ratio are inelastic H^+–H_2 and H–H_2 collisions, which determine the interconversion of *ortho*- and *para*-H_2 at low and high temperatures, respectively. The introduction of recently calculated values of the rate coefficients for these collision processes should ensure the accuracy of the computed data. At temperatures $T \lesssim 100$ K or densities $n_\mathrm{H} \gtrsim 10^6$ cm^{-3}, the level populations approach their values in thermodynamic equilibrium, which greatly simplifies the evaluation of the level populations and the cooling rate.

ACKNOWLEDGEMENTS

This project received funding from the European Research Council (ERC) under the European Union's Horizon 2020 research and innovation programme (grant agreement no. 811363). We acknowledge the Programme National Physique et Chimie du Milieu Interstellaire (PCMI) of CNRS/INSU with INC/INP co-funded by CEA and CNES. FL acknowledges financial support from the Institut

Universitaire de France. TG-L acknowledges support from project no. FIS2017-83157-P (MINECO/AEI/FEDER, UE). DRF acknowledges support from STFC (ST/L00075X/1), including provision of local computing resources.

DATA AVAILABILITY

The data generated by this study are available as supplementary online material.

REFERENCES

Abgrall H., Roueff E., 1989, A&AS, 79, 313
Anders E., Grevesse N., 1989, Geochim. Cosmochim. Acta, 53, 197
Coppola C. M., Kazandjian M. V., Galli D., Heays A. N., van Dishoeck E. F., 2017, MNRAS, 470, 4163
Coppola C. M., Lique F., Mazzia F., Esposito F., Kazandjian M. V., 2019, MNRAS, 486, 1590
Courtney E., Stancil P., McArdle R., Forrey R., Babb J., 2020, BAAS, 52, 236
England J. P., Elford M. T., Crompton R. W., 1988, Aust. J. Phys., 41, 573
Flower D. R., Le Bourlot J., Pineau des Forêts G., Roueff E., 2000, MNRAS, 314, 753
Flower D. R., Pineau des Forêts G., 2000, MNRAS, 316, 901
Flower D. R., Pineau des Forêts G., 2001, MNRAS, 323, 672
Galli D., Palla F., 1998, A&A, 335, 403
Gear C. W., 1971, Numerical Initial Value Problems in Ordinary Differential Equations. Prentice-Hall, Englewood Cliffs, NJ
Gerlich D., 1990, J. Chem. Phys., 92, 2377
Glover S. C. O., 2015, MNRAS, 451, 2082
Glover S. C. O., Abel T., 2008, MNRAS, 388, 1627
González-Lezana T., Hily-Blant P., Faure A., 2021, J. Chem. Phys., 154, 054310
Hernández M. I., Tejeda G., Fernández J. M., Montero S., 2021, A&A, 647, A155
Le Bourlot J., Pineau des Forêts G., Flower D. R., 1999, MNRAS, 305, 802
Le Petit F., Nehmé C., Le Bourlot J., Roueff E., 2006, ApJS, 164, 506
Lee T.-G., Balakrishnan N., Forrey R. C., Stancil P. C., Shaw G., Schultz D. R., Ferland G. J., 2008, ApJ, 689, 1105
Lique F., 2015, MNRAS, 453, 810
Montero S., Tejeda G., Fernández J. M., 2020, ApJS, 247, 14
Pachucki K., Komasa J., 2008, Phys. Rev. A, 77, 030501
Pitrou C., Coc A., Uzan J.-P., Vangioni E., 2018, Phys. Rep., 754, 1
Puy D., Alecian G., Le Bourlot J., Léorat J., Pineau des Forêts G., 1993, A&A, 267, 337
Ripamonti E., Abel T., 2004, MNRAS, 348, 1019
Walker K. M., Porter R. L., Stancil P. C., 2018, ApJ, 867, 152
Wan Y., Yang B. H, Stancil P. C., Balakrishnan N., Parekh N. J., Forrey R. C., 2018, ApJ, 862, 132

SUPPORTING INFORMATION

Supplementary data are available at *MNRAS* online.

interpolation.f90, interp.inp, and grille_W_1

Please note: Oxford University Press is not responsible for the content or functionality of any supporting materials supplied by the authors. Any queries (other than missing material) should be directed to the corresponding author for the article.

APPENDIX:

In Fig. A1, we compare our computed cooling function, W, with the fits of Glover & Abel (2008) and Glover (2015) for the cases in which H or H^+ and, at high T, electron collisions dominate. In our calculations, the gas density $n_H = 1$ cm$^{-3} \approx n$(H) or $n(H^+)$, respectively. The comparisons are rendered inexact by the fact that we do not assume a constant *ortho*:*para* ratio of 3. As may be seen in the upper panel of the figure, the rates of cooling by H^+ agree well for $T \approx 10^3$ K but diverge at lower and, to a lesser degree, higher temperatures. At low T, the cooling is dominated by quadrupole transitions between the lowest rotational states of H_2, for which the low-density limit – assumed in the fits of Glover (2015) – is not attained when $n_H = 1$ cm^{-3}. On the other hand, when H collisions dominate, the low-density limit applies even at low temperatures, and the results for *para*-H_2–H cooling agree reasonably well; *para*-H_2 is the principal form of molecular hydrogen at low T, in steady state.

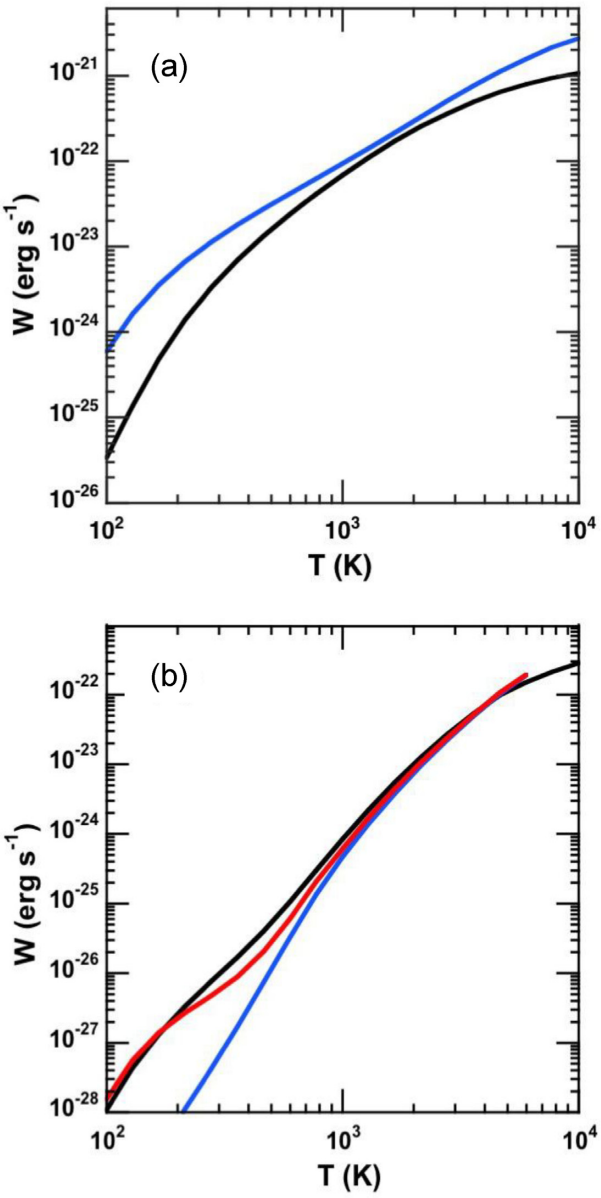

Figure A1. Comparing the cooling rate of molecular hydrogen in the cases in which (a) H^+ and e^- collisions dominate, or (b) H collisions dominate. The comparisons are made with the fits of Glover (2015) (blue curve in panel a) and Glover & Abel (2008) (blue curve in panel b for *ortho*-H_2 and red curve for *para*-H_2). The black curves are the present results for a gas density $n_H = 1$ cm^{-3} (see the text).

This paper has been typeset from a TEX/LATEX file prepared by the author.